Creeping flows of Bingham fluids through arrays of aligned cylinders

P. D. M. Spelt[1], A. Y. Yeow[1], C. J. Lawrence[1] and T. Selerland[2]

[1] *Department of Chemical Engineering, Imperial College London, U.K.*
[2] *CFD Recipes, 39 High Street Chesterton, Cambridge, U.K.*

Abstract

Numerical simulations are presented for flows of Bingham fluids through periodic square arrays of aligned cylinders, for cases in which fluid inertia can be neglected. The aim is to quantify the dependence of the drag coefficient of the cylinders on the Bingham number. The results for large Bingham numbers, and also for dilute arrays of cylinders (low solid area fraction) are shown to approach previous analytical results for a single cylinder. The results for concentrated arrays are shown to agree with a lubrication theory. Although the rheology is strongly nonlinear and significant unyielded regions are shown to develop, the drag coefficient is approximately a linear function of the Bingham number. This is shown to be the case for flows along a principal axis of the array and also seems to hold for flow at 45 degrees (in the plane perpendicular to the cylinders). It is shown that the drag force on a cylinder in the array immersed in a Bingham fluid is approximately equal to the sum of the drag forces in the corresponding cases of Newtonian and perfectly plastic fluids. This result is used to derive a criterion for the critical pressure gradient, required for flow. Implications for large-scale modeling of flow through fibrous media are discussed.

Key words: Bingham fluids; creeping flow; periodic arrays

1 Introduction

The flow of Newtonian fluids through periodic arrays of aligned cylinders has been studied extensively for a range of applications (*e.g.*, [1,2]), varying from heat exchangers to the glycocalyx layer on the surface of cells. The corresponding flows of non-Newtonian fluids are of interest, for instance, as a model problem for enhanced oil recovery, paper pressing and resin transfer moulding applications. Studies on flows of non-Newtonian fluids have primarily elucidated the roles of shear-thinning (or shear-thickening) rheological behaviour

[3–9] and viscoelasticity (with emphasis on the development of elastic instabilities, see, *e.g.*, [10]).

Less well documented is the flow through porous or fibrous media of materials that exhibit a transition between 'solid' and 'liquid'-type rheological behaviour (and vice versa). A well-established model for such behaviour is that of a Bingham material, in which a discrete transition stress value (the yield stress) distinguishes between the two types of behaviour. Although this concept has been the subject of vigorous debate (leading for instance to the important suggestion that transition occurs not at a discrete yield stress, but over a range of stress values), it remains a very useful approximation (a recent brief review and detailed measurements are available in [11]). Previous work include studies on the flow past a falling sphere [12], flow past a single cylinder [13,14] and squeezing flows (see, *e.g.*, [15] and references therein). In most numerical studies, the exact Bingham rheological model is replaced by a regularized model, that allows *a posteriori* determination of the yield surface, and the use of a single rheological description throughout the entire domain. Regularizations include the bi-viscosity model [16–20]. and the Papanastasiou model [14,21,22]. The former will be used in this study (it is introduced in Section 2 below).

For the present application it is clear that a minimum (or critical) pressure gradient across a porous medium is required for flow of a Bingham material to occur. A previous study by Nieckele *et al.* [23] confirms this, and shows the location of unyielded zones and the tendency towards plug flow as the yield stress is increased. But it has not been shown how the critical pressure gradient can be predicted from an explicit relationship, or how the pressure gradient across a porous medium is related to the flow rate: the previous work by Nieckele *et al.* is primarily qualitative in nature. The determination of such relationships is essential for the development of an accurate description of complex large-scale flows of such fluids through porous media. A main outcome of the previous work on inelastic shear-thinning fluids cited above is that, for several cylinder arrangements and a range of flow angles, the results for shear-thinning and shear-thickening fluids can be expressed in terms of those for the corresponding Newtonian fluid flow, resulting in a modified Darcy's law (this is discussed in detail in [7,9]; see also Section 3.4 below). Woods *et al.* [9] showed that similar conclusions hold for flow through arrays of elliptical cylinders. This outcome of previous work can be used further to understand and model flows of shear-thinning fluids with a significant low-shear-rate Newtonian plateau (in the viscosity vs shear rate curve), as shown in [7], and flows of shear-thinning fluids with inertia [8]. The present paper aims to provide a similar level of understanding and modelling of corresponding flows of Bingham fluids.

Therefore, in this paper we present a quantitative investigation of the flow of a fluid with a yield stress through a periodic array of cylinders. This study

addresses the main problem of steady creeping flow in the plane perpendicular to a square array of cylinders, with the flow directed along one of the principal axes of the array. This is motivated by previous work on shear-thinning fluids [7–9], which shows that results for a variety of other flows can be related to this basic flow. Some results will be presented for flow directed at an angle of 45 degrees with respect to the main axis of the array (in the plane perpendicular to the cylinders), these will prove to be very similar.

The main dimensionless parameters are the solid area fraction ϕ and the dimensionless yield stress, or Bingham number

$$Bn \equiv a\tau_0/(\mu_B U), \tag{1}$$

where a is the radius of the cylinders, τ_0 is the yield stress, μ_B is the Bingham viscosity and U is the cell-averaged fluid velocity (which is the velocity component in the main flow direction averaged over the total area of the array, including the space occupied by the cylinders, where the velocity is taken to be zero). The numerical method to solve the equations of motion of the bi-viscosity model is essentially the same as that presented in [7], the adaptations made are provided in Section 2, together with convergence tests. Results are presented for large ranges of ϕ and Bn in Section 3. A main objective is to determine the functional dependence of the drag coefficient of a cylinder in the array on Bn (Sections 3.3 and 3.4). These results are used subsequently to determine the critical pressure gradient required for flow to occur (Sec. 3.5).

2 Equations of motion and numerical method

If the magnitude of the deviatoric stress exceeds the yield stress, the Bingham material yields and behaves like a non-Newtonian fluid. The yield criterion is that the second invariant $\Pi_\tau \equiv (\frac{1}{2}\tau_{kl}\tau_{kl})^{1/2}$ of the deviatoric stress tensor τ_{ij} exceeds the yield stress, τ_0. For yielded material, the deviatoric stress tensor τ_{ij} is related to the rate-of-strain tensor $E_{ij} = \frac{1}{2}\left(\partial u_i/\partial x_j + \partial u_j/\partial x_i\right)$ through

$$\tau_{ij} = 2\left(\mu_B + \tau_0\Pi^{-1}\right)E_{ij} = 2\mu_A E_{ij} \qquad (\Pi_\tau > \tau_0), \tag{2}$$

where $\Pi \equiv (2E_{kl}E_{kl})^{1/2}$ is the second invariant of the rate-of-strain tensor and μ_A is the apparent viscosity. In the unyielded zones the Bingham material behaves as a rigid solid:

$$E_{ij} = 0 \qquad (\Pi_\tau \leq \tau_0). \tag{3}$$

(see [24] for a review). The numerical representation of this rheological model is complicated mainly by two factors. First, by the difference in behaviour of the material in the yielded and unyielded regions. Second, by the fact that

the position of the yield surface (i.e., the surface along which $\Pi_\tau = \tau_0$) should be tracked, although this is not a material surface; this was done by Beris *et al.* [12] for flow past a sphere. In order to overcome both of these problems, a modification of the Bingham model is usually adopted. We shall use here the bi-viscosity model [16–20], corresponding to imposing a maximum value on the apparent viscosity to be used in (2), with the additional requirement that this maximum viscosity is sufficiently large that its value does not affect the results. So the unyielded material is made into a very viscous fluid, rather than a solid. The transition between the two types of behaviour occurs at $\Pi_\tau = \mu_{\max}\tau_0/(\mu_{\max} - \mu_B)$. We introduce the regularization parameter

$$R = \frac{\mu_{\max}}{\mu_B}. \tag{4}$$

The Bingham material is recovered in the limit $R \to \infty$ for a given finite value of Bn. We present results in the next section to show that the values of R used in our calculations were sufficiently large to give a close approach to this limit.

We have solved the creeping flow equations using the finite-difference, fractional step method presented in [7] for body-fitted grids, based on the method of Zang *et al.* [25] for Newtonian fluids. The same code (but with $\mu_A = \mu_B + \tau_0/\Pi$ as the apparent viscosity) has been used to numerically simulate the flow of creeping flows of inelastic non-Newtonian fluids through arrays of circular cylinders [7], and the creeping flows of power-law fluids through arrays of elliptical cylinders [9].

The equations of motion were solved for a unit cell of the array, using periodic boundary conditions. No-slip boundary conditions were used at the surface of the cylinder. A pressure drop was imposed over the unit cell by making the pressure on the right surface of the cell (through which the fluid leaves) equal to that on the left surface (through which the fluid enters) minus the prescribed pressure drop Δp. A similar approach was adopted for the bottom and top surfaces for flows at 45 degrees. The main result from each calculation is the cell-averaged velocity U, which is obtained by integrating the component of velocity in the main flow direction over the entire cell, using zero velocity inside the cylinders. We note here that, consequently, the Bingham number is not an input parameter. In each simulation Δp, μ_B, R and τ_0 were chosen and Bn was calculated a posteriori.

3 Results

3.1 Effect of regularization parameter and mesh size

Results for the cell-averaged velocity U are presented for different values of the regularization parameter R in Table 1. Results are included for three different mesh sizes ($32 \times 30, 42 \times 40$ and 62×60) to show the convergence with respect to discretization error. The solid area fraction ϕ was 0.1 in all cases included in Table 1. We see that for each mesh, U converges as R is increased. The resulting values of U correspond to $Bn = 1.25 \pm 0.01$ or 4.28 ± 0.03 (which therefore converge as part of the solution). The dominant source of error is seen to be not due to the regularization parameter, but due to the mesh size. The discretization error in U is smaller than 1% for the two largest meshes, and converges with mesh size.

The steady-state results were obtained from a time-integration from rest, so there is an effect of the timestep on the results. In most cases, the timestep used was $\Delta t \sim R^2$, but the timestep was decreased for larger meshes, $\Delta t \sim N^{-2}$ (where N is the number of mesh points in each direction). The results for $Bn = 1.25 \pm 0.01$ in Table 1 were obtained using these rules, with $\Delta t = 8 \cdot 10^{-4}$ for the 32×30 mesh at $R = 14$. The dependence of U on R shown may be partly influenced by the timestep used. The calculation for the largest value of R and largest mesh size shown took over $9 \cdot 10^5$ timesteps to approach the steady state sufficiently closely. We have verified that for the calculations presented below the change in U after doubling R was less than 1%. A 62×60 mesh has been used in all subsequent simulations. The convergence of the shape of yield surfaces is discussed in the next subsection.

3.2 Yield surfaces

In Figure 1, the surfaces at which $\Pi_\tau = \tau_0$, which are an approximation of the yield surfaces, are shown for $Bn = 4.28 \pm 0.03$, for $\phi = 0.1$ and for different values of R. The flow is from left to right. The yield surfaces were obtained from the simulation data using third-order interpolation. Unyielded regions are found around the points of symmetry; a large unyielded region occurs in the narrowest part of the gap between the cylinders. Even at this relatively low value of ϕ ($= 0.1$), the locations of the unyielded zones are different from those for a single cylinder. De Besses *et al.* [14] showed that there are triangular unyielded zones at the stagnation points, as well as small regions close to the cylinder top and bottom. The latter are located approximately at the same place as the upper and lower part of the large central region in Figure 1,

but the former are absent in the present results. Although the presence of the up- and downstream cylinders causes a significant disturbance in the unit cell of the periodic array, insufficient numerical resolution could be a factor. The calculation of Π_τ requires the velocity components of neighbouring cells, and the wedges at stagnation points are possibly too small for the present calculations to capture (a local maximum in μ_A at stagnation points is observed in the data, also in off-axis flow).

The loci of the yield surfaces in Figure 1, in the corners of the domain and parts of the surfaces in the middle left and right, have just about converged for the largest value of R shown. The locus of the large yield surface in the centre of the domain is converging more slowly. In order to obtain fully converged yield surfaces, the value of R would need to be larger, which would require a very small timestep ($\Delta t \sim R^2$), and excessive computational time. This does not significantly affect the results for the mean velocity, however, as is apparent from Table 1; the value of U has converged to within 1% for the largest value of R.

Yield surfaces for the largest value of ϕ simulated here ($\phi = 0.6$) can be inferred from the iso-viscosity contours shown in Figure 2a,b. These figures are for small and large values of Bn, respectively. The flow is from left to right. The viscosity is seen to vary rapidly close to unyielded zones, but slowly elsewhere. Although the yield surface locations are similar to those in Figure 1, the unyielded regions in the corners of Figure 2 are seen to touch the cylinder surfaces, and to consist of the entire regions between neighbouring (up- and downstream) cylinders. The size of these latter regions appears to be only weakly dependent on the value of Bn, whereas the other regions grow significantly with Bn.

3.3 Drag coefficient

The pressure drop applied across the unit cell is balanced by the drag force on the cylinders. This force balance over the unit cell has been used to obtain the drag coefficient (alternatively, a modification of Darcy's law can be obtained; the drag coefficient is related inversely to the effective permeability coefficient, as is discussed in [9]; see also the conclusions section below). As a result of dimensional analysis, we can introduce a drag coefficient C_d by writing, for the limit $R \to \infty$ considered here,

$$F \equiv C_d(\phi, Bn)\mu_B U, \tag{5}$$

where F is the applied force per unit length of cylinder. F is the product of the applied pressure drop over the cell and the length of the side of the cell, and is therefore known; the cell-averaged velocity U is obtained from the

simulations, and the drag coefficient is obtained from (5).

Results for C_d as a function of Bn are shown in Figure 3 for a range of solid volume fractions (0.01-0.6). All of the simulation results approach the corresponding Newtonian value for $Bn = 0$ (indicated by the dotted lines), as required. We found the results for $Bn = 0$ to agree within 1% with those previously published by Sangani and Acrivos [1].

The results for dilute arrays at intermediate values of Bn are seen to be close to the approximate results for a single cylinder (obtained by a variational method by Adachi and Yoshioka [13]), and a fit of more recent simulations for a single cylinder by De Besses *et al.* [14]. (It should be noted that the numerical approximations made by Adachi and Yoshioka [13] are crude, and that De Besses *et al.* [14] used the Papanastasiou model.)

At large Bn, most results appear to converge to an analytical asymptotic result for a single cylinder, obtained from a slip-line analysis [13]:

$$C_d \approx (2\pi + 4)\, Bn \qquad \text{(single cylinder)}. \tag{6}$$

This is only an approximate result, because Adachi & Yoshioka [13] assumed a simple yield surface and only took pressure variations into account, but the simulations of De Besses *et al.* [14] also show reasonable agreement. If Bn is sufficiently large, the fluid is expected to yield only in a small region around each cylinder as if each cylinder is isolated. We shall discuss in the next section the case of relatively large ϕ, where the cylinders are very close together (this will be of interest because the numerical results for concentrated arrays appear not to converge exactly to (6)).

In Figure 4 the same results are used to plot the difference between $C_d(\phi, Bn)$ and its corresponding value $c_0(\phi, Bn = 0)$ for a Newtonian fluid (of viscosity μ_B). Remarkably, close inspection of this graph shows that we can write a simple approximation

$$C_d(\phi, Bn) \approx c_0(\phi) + c_1(\phi) Bn. \tag{7}$$

We see that c_1 does not depend strongly on ϕ for intermediate values of ϕ, the data almost collapse onto a single line. Results are also shown for flow directed at an angle of 45 degrees with respect to the main axis of the array (in the plane perpendicular to the cylinders), at $\phi = 0.3$. Here, U in the definition of Bn and C_d is replaced by $\sqrt{U_1^2 + U_2^2}$, where U_i is the cell-averaged fluid velocity component in the $i-$direction. The results for off-axis and on-axis flow are seen to be very similar.

For very small values of Bn, the right-hand side of (7) could be regarded as the first two terms of a Taylor series expansion in Bn, with the first term

corresponding to a Newtonian fluid ($Bn = 0$). However, the results presented here extend far beyond a small perturbation to the Newtonian fluid. The range of Bn for which results are presented here is significant: the drag coefficient changes in this range by at least a factor of two for all solid fractions, and the unyielded regions are found to be substantial (this is discussed further in section 3.4 below). For the range of values of Bn covered by the present simulations, we did find a weak deviation from (7) as Bn was increased. Moreover, the second term on the right-hand-side of (7) becomes significant even at small values of Bn in the case of dilute arrays.

We have obtained the coefficient c_1 as a function of solid fraction as the linear coefficient in a second-order polynomial fit to the simulation data shown in Figure 4. The results are dominated by the smaller values of Bn, such that omitting the data point at the largest value of Bn for each solid fraction resulted in a change in c_1 of less than 2%. The results are shown by square symbols in Figure 5. The value for c_1 for the results shown in Figure 4 for flow at 45 degrees with $\phi = 0.3$ is approximately 24.5, which is quite close to the corresponding on-axis result of 22.2. A strong increase in c_1 is seen at low and high solid fractions. We also see that all values are significantly above the approximate result (6) for a single cylinder, which was derived for large Bn. For $\phi = 0.1$, relatively large values of Bn were simulated, and from Figure 3 it is seen that higher-order corrections to (7) would result in a closer agreement with (6).

Some insight into these results can be obtained by observing that (7) is approximately valid for any value of Bn, and investigating the case of large Bn to obtain an approximation for c_1. At large Bingham numbers, one expects the apparent viscosity to be dominated by $\tau_0 \Pi^{-1}$ (cf. (2)). Neglecting the Bingham viscosity in (2) everywhere amounts to supposing the material to be perfectly plastic, which corresponds to the limit of a power-law fluid with power-law index equal to zero. We shall now investigate under what circumstances this is a good approximation. In [7] results have been presented for flows of power-law fluids through arrays of cylinders. For power-law fluids, (2) is replaced by

$$\tau_{ij} = K \Pi^{n-1} E_{ij}, \tag{8}$$

where K and n are the power-law coefficient and index, respectively, and the drag coefficient $\hat{C}_d$ is defined by

$$F \equiv \hat{C}_d(\phi, n) K a^{1-n} U^n. \tag{9}$$

Although the numerical simulations presented in [7] do not extend down to $n = 0$, a very simple scaling relation was found for the drag coefficient which

we shall use here to extrapolate the results for $\hat{C}_d$ to $n = 0$:

$$\hat{C}_d(\phi, n) = \hat{C}_d(\phi, 1) \left(\frac{\phi}{\phi_{\max}} \right)^{(1-n)/2} \left(\frac{\mathcal{L}}{a} \right)^{2-2n}, \tag{10}$$

where $\mathcal{L}/a$ depends on the solid fraction and $\phi_{\max}$ is the maximum solid fraction ($\phi_{\max} = \pi/4$ for square arrays). $\hat{C}_d(\phi, 1)$ is the drag coefficient for a Newtonian fluid, corresponding to $c_0(\phi)$ in (7). The results presented in [7] show that $\mathcal{L}$ is approximately equal to half the minimum distance between the cylinders, L_g, if ϕ is not very small. For square arrays, $L_g/a = (\phi_{\max}/\phi)^{1/2} - 1$.

Returning to the case of Bingham fluids, we see that neglecting μ_B in (2) corresponds to a power-law fluid with $n = 0$ and $K = \tau_0$, while the drag coefficients are related by $C_d = \hat{C}_d(\phi, n = 0)Bn$. Hence we find the approximation

$$c_1(\phi) \approx \hat{C}_d(\phi, n = 0) \approx c_0(\phi) \left(\frac{\phi}{\phi_{\max}} \right)^{1/2} \left(\frac{\mathcal{L}}{a} \right)^{2} \equiv \hat{c}_1. \tag{11}$$

In Figure 5 we compare the results for c_1 as a function of solid fraction with $\hat{c}_1$ given by (11). In the determination of $\hat{c}_1$, we have used the numerical results in [7] for the ratio $\mathcal{L}/a$ in (11). Alternatively, the reasonable approximation $\mathcal{L} = L_g$ could have been used (it was found that this would have resulted in a small shift upwards of the results in Figure 5, closer to the results for c_1). We see that for $0.1 < \phi < 0.3$, $\hat{c}_1$ is close to c_1, although consistently smaller; but for dilute and concentrated arrays c_1 becomes significantly larger than $\hat{c}_1$. We have also plotted in Figure 5 a lubrication theory for perfectly plastic materials derived in [7] (their equation (15)),

$$\hat{c}_1^{\text{lub}} = 2^{3/2}\pi \left(1 - \left(\frac{\phi}{\phi_{\max}} \right)^{1/2} \right)^{-1/2}, \quad (\, |\phi - \phi_{\max}| \ll 1), \tag{12}$$

which is seen to agree well with the result (11), supporting the extrapolation procedure adopted here to obtain $\hat{C}_d$ for $n = 0$.

The expression (7), when c_1 is approximated by $\hat{c}_1$ given in (11), corresponds to writing the total drag force on a cylinder in a Bingham fluid as the sum of the forces corresponding to Newtonian fluid and perfectly plastic fluid, respectively. We conclude from the reasonable agreement between c_1 and $\hat{c}_1$ in Figure 5 that this is a reasonable approximation, especially at intermediate solid fractions.

In order to explain the difference between the numerical simulations and the approximation (11) at relatively large values of ϕ, we derive here a lubrication theory for Bingham fluids.

Adopting the bi-viscosity model, it is straightforward to derive the velocity profile in the narrow gap between the cylinders using standard lubrication theory arguments. Denoting the coordinate in the flow direction by x (with $x = 0$ corresponding to the point where the gap size reaches its smallest value) and the cross-flow coordinate by y ($y = 0$ corresponding to the symmetry axis), the result is (for $y \geq 0$)

$$u(y) = \begin{cases} \mathcal{U}(x) + 2^{-1}\mu_{\max}^{-1}\,(dp/dx)\,y^2 & (y \leq y_0), \\ -2^{-1}\mu_B^{-1}\,(dp/dx)\,(h^2 - y^2) - \mu_B^{-1}\tau_0\,(h - y) & (y \geq y_0), \end{cases} \tag{13}$$

in which $\mathcal{U}(x) = -\frac{1}{2}(dp/dx)(h^2 - y_0^2(1 - \mu_B/\mu_{\max}))/\mu_B - \tau_0(h - y_0)/\mu_B$ is a slowly varying "plug" velocity that is obtained from continuity of u at the yield surface $y = y_0(x)$, and $h(x)$ is half the gap size.

In a "naive" approach, the yield surface location y_0 would be obtained from the yield condition,

$$\tau_0 = -y_0\frac{dp}{dx}. \tag{14}$$

But this is only correct if normal stresses can be ignored compared to shear stresses in the "unyielded" region. From the full two-dimensional yield criterion and (13) it can be shown that this restricts the analysis to the case $\mu_{\max}/\mu_B \ll (a/h)^{1/2}$ (see also [20,26]).

An equation for the pressure gradient can be obtained by integrating (13) over the cross-section, equating the result to the ($x-$independent) flux through half the gap, Uc (c is half the distance between the centres of two neighbouring cylinders), and taking the limit $\mu_B/\mu_{\max} \to 0$:

$$P^3 + 3\left(\mathcal{B}^{-1} + \frac{1}{2}\right)P^2 - \frac{1}{2} = 0, \tag{15}$$

with $P \equiv (h/\tau_0)(dp/dx)$ and $\mathcal{B} \equiv \tau_0 h^2/(\mu_B U c) = h^2 Bn/(ac)$.

In the limit of concentrated arrays, $\mathcal{B}$ is a small parameter unless Bn is extremely large, which was not the case in the numerical simulations. For small values of $\mathcal{B}$, the solution of (15) is

$$P = -3\mathcal{B}^{-1} - \frac{3}{2} + O(\mathcal{B}^2). \tag{16}$$

The drag coefficient can now be obtained from integrating the pressure gradient with respect to x. The first two terms on the r.h.s. of (16) result in a drag coefficient that can be written in the form of (7) with

$$c_1^{\mathrm{lub}} = \frac{3}{2}\hat{c}_1^{\mathrm{lub}}, \tag{17}$$

where $\hat{c}_1^{\mathrm{lub}}$ is given by (12). This result is indicated by a solid line in Figure 5. The data for c_1 are seen to approach (17) for large values of ϕ. This is surprising, because the lubrication theory is valid only for $\mu_{\max}/\mu_B \ll (a/h)^{1/2}$, whereas in the simulations, the limit $\mu_B/\mu_{\max} \to 0$ is taken for a given value of ϕ; the convergence of all results with respect to the value of $\mu_{\max}$ has been tested. The results suggest therefore that the order in which the two limits are taken is not important.

In the limit of large values of $\mathcal{B}$ it can be shown that to leading order $P = -1$, which leads to $c_1^{\mathrm{lub}} = \hat{c}_1^{\mathrm{lub}}$, as required. The difference between the data for c_1 and the approximation (11) at large solid fractions arises because very large values of Bn are required in order to approach the perfect-plastic regime for concentrated arrays (which would lead to a deviation from (7)).

3.5 Critical pressure gradient

A minimum (or critical) pressure gradient is of course required for a Bingham fluid to flow through the array. In Figure 6 the superficial fluid velocity is shown as a function of the pressure gradient across the array, $G = \Delta p/(2c)$, where Δp is the pressure drop over the unit cell. Beyond the critical pressure gradient, the velocity is seen to gradually approach the Newtonian fluid value (as the regions where the stress is close to the yield stress shrink to zero). The critical pressure gradient is seen to increase with solid area fraction. The results presented by Nieckele *et al.* [23] are qualitatively similar, although a different geometry was considered.

It is clear from Figure 6 that values of Bn larger than those for which results have been presented above occur only in a very small range of G, just beyond the onset of flow. Hence it must be possible to obtain from (7) (which represents the results presented so far) an accurate prediction of the critical pressure gradient. The definition of the drag coefficient (5) can be written explicitly in terms of the pressure drop across a unit cell of the array:

$$\frac{\Delta p}{\tau_0} = \frac{1}{2}C_d(\phi, Bn)\left(\frac{\phi}{\phi_{\max}}\right)^{1/2} Bn^{-1}. \tag{18}$$

Upon substitution of the approximation (7), we have

$$\frac{U(Bn)}{U(0)} \approx 1 - \left(\frac{2cG_{\rm crit}}{\tau_0}\right)\frac{\tau_0}{2cG}, \tag{19}$$

with the critical dimensionless pressure gradient

$$\frac{2cG_{\rm crit}}{\tau_0} = \frac{1}{2}c_1(\phi)\left(\frac{\phi}{\phi_{\rm max}}\right)^{1/2}. \tag{20}$$

The left-hand side of (19) is the ratio of the superficial fluid velocity to the corresponding value for a Newtonian fluid at the same pressure gradient ($U(0) = 2c\Delta p/(C_d(\phi,0)\mu_B)$). This result is also shown in Figure 6 (as the solid lines), and is seen to be a good approximation, even quite close to the critical value of $2cG/\tau_0$. Details of the unyielded regions just beyond the onset of flow cause the drag to be larger than (7), so that (20) is a slight overestimate.

4 Conclusions

Numerical simulation data have been presented for the flow of Bingham fluids through periodic arrays of cylinders. The rheology of the fluids was regularized using a bi-viscosity model. The cell-averaged fluid velocity is shown to converge for sufficiently small values of the regularization parameter, although the shape and position of (the approximations of) the yield surfaces may not have precisely converged for the largest values of Bn simulated.

The drag coefficient C_d of a cylinder is shown to depend approximately linearly on the Bingham number (*cf.* (7)), where $Bn = 0$ corresponds to a Newtonian fluid. This is the case for flow directed along an axis of the array and at 45 degrees (in the plane perpendicular to the cylinders). The results show that the drag force on a cylinder in a Bingham fluid can be approximated by the sum of the drag forces in the corresponding cases of Newtonian and perfectly plastic fluids. Some deviation from this approximation occurs in concentrated arrays. We present a lubrication theory which indicates that convergence to the result for perfectly plastic fluids can be obtained only for very large values of the Bingham number. The approximation (7) is used in Sec. 3.5 to derive a criterion for the onset of flow through an array.

The present results suggest a particular Darcy-type formulation for flow of Bingham fluids through fibrous media. On a large scale, the pressure gradient across an array of cylinders is balanced by the drag forces exerted by the cylinders. Substitution of (5) for the drag on a single cylinder in the array

leads to the Darcy-type law,

$$\frac{\partial p}{\partial x} = -K^{-1}(\phi, Bn)\mu_B U, \tag{21}$$

where $K(\phi, Bn) = (\phi/(\pi a^2))C_d^{-1}(\phi, Bn)$ is the effective permeability. The results presented in this paper show that, for flow perpendicular to the axis of the cylinders, along an axis of the array, the approximation

$$K(\phi, Bn) \approx \frac{\phi}{\pi a^2}\left(C_d(\phi, 0) + c_1(\phi)Bn\right)^{-1} \tag{22}$$

may be used, with $c_1(\phi)$ given by (11) (for intermediate ϕ) or (17) (for large ϕ). The close agreement between results for flow along an axis of the array and at 45 degrees suggests that, for arbitrary off-axis flow at intermediate ϕ, the components of the pressure gradient also satisfy (21) (with K approximately equal to its on-axis value), if U in the right-hand-side of (21) is replaced by the corresponding component of the cell-averaged velocity vector, and U in the definition of Bn by the magnitude of the cell-averaged velocity vector.

This work was made possible by a grant from EPSRC (GR/M 39572) and was supported by QinetiQ, Vosper Thornycroft, Dowty Aerospace Propellers, AEA Technology and BAE Systems. PDMS would like to acknowledge the use of computational facilities at the School of Mathematical Sciences of the University of Nottingham.

References

[1] A. S. Sangani and A. Acrivos, Slow flow past periodic arrays of cylinders with application to heat transfer. Int. J. Multiphase Flow 8 (1982), 193-206.

[2] D. L. Koch and A. J. C. Ladd, Moderate Reynolds number flows through periodic and random arrays of aligned cylinders. J. Fluid Mech. 349 (1997), 31-66.

[3] M. V. Bruschke and S. G. Advani, Flow of generalized Newtonian fluids across a periodic array of cylinders. J. Rheol. 37 1993, 479-498.

[4] B. N. Dhotkar, R. P. Chhabra and V. Eswaran, Flow of non-Newtonian polymeric solutions through fibrous media. J. Appl. Polym. Sci. 76 (2000), 1171-1185.

[5] Z. Idris, L. Orgeas, C. Geindreau, J. F. Bloch and J. L. Auriault, Microstructural effects on the flow law of power-law fluids through fibrous media. Model. Sim. Mat. Sci. Eng. 12 (2004), 995-1015.

[6] D. V. N. Prasad and R. P. Chhabra, An experimental investigation of the cross-flow of power-law liquids past a bundle of cylinders and in a bed of stacked screens. Can. J. Chem. Eng. 79 (2001), 28-35.

[7] P. D. M. Spelt, T. Selerland, C. J. Lawrence and P. D. Lee, Flows of inelastic non-Newtonian fluids through arrays of aligned cylinders. Part 1. Creeping flows. J. Eng. Math. 51 (2005), 57-80.

[8] P. D. M. Spelt, T. Selerland, C. J. Lawrence and P. D. Lee, Flows of inelastic non-Newtonian fluids through arrays of aligned cylinders. Part 2. Inertial effects for square arrays. J. Eng. Math. 51 (2005), 81-97.

[9] J. K. Woods, P. D. M. Spelt, T. Selerland, C. J. Lawrence and P. D. Lee, Creeping flows of power-law fluids through a periodic array of elliptical cylinders. J. Non-Newt. Fluid Mech. 111 (2003), 211-228.

[10] B. Khomami and L. D. Moreno, Stability of viscoelastic flow around periodic arrays of cylinders. J. Non-Newt. Fluid Mech. 36 (1997), 367-383.

[11] P. H. T. Uhlherr, J. Guo, C. Tiu, X.-M. Zhang, J. Z.-Q. Zhou and T.-N. Fang, The shear-induced solid-liquid transition in yield stress materials with chemically different structures. J. Non-Newt. Fluid Mech. 125 (2005), 101-119.

[12] A. N. Beris, J. A. Tsamopoulos, R. C. Armstrong and R. A. Brown, Creeping motion of a sphere through a Bingham plastic. J. Fluid Mech. 158 (1985), 219-244.

[13] K. Adachi and N. Yoshioka, On creeping flow of a visco-plastic fluid past a circular cylinder. Chem. Eng. Sci. 28 (1973), 215-226.

[14] B. D. De Besses, A. Magnin and P. Jay, Viscoplastic flow around a cylinder in an infinite medium. J. Non-Newt. Fluid Mech. 115 (2003), 27-49.

[15] D. N. Smyrnaios and J. A. Tsamopoulos, Squeeze flow of Bingham plastics. J. Non-Newt. Fluid Mech. 100 (2001), 165-190.

[16] M. Bercovier and M. Engelman, A finite-element method for incompressible non-Newtonian flows. J. Comp. Phys. 36 (1980), 313-326.

[17] G. G. Lipscomb and M. M. Denn, Flow of Bingham fluids in complex geometries. J. Non-Newt. Fluid Mech. 14 (1984), 337-346.

[18] B. T. Liu, S. J. Muller and M. M. Denn, Convergence of a regularization method for creeping flow of a Bingham material about a rigid sphere. J. Non-Newt. Fluid Mech. 102 (2002), 179-191.

[19] E. J. O'Donovan and R. I. Tanner, Numerical study of the Bingham squeeze film problem. J. Non-Newt. Fluid Mech. 15 (1984), 75-83.

[20] S. D. R. Wilson, Squeezing flow of a Bingham material. J. Non-Newt. Fluid Mech. 47 (1993), 211-219.

[21] E. Mitsoulis and R. R. Huilgol, Entry flows of Bingham plastics in expansions. J. Non-Newt. Fluid Mech. 122 (2004), 45-54.

[22] T. C. Papanastasiou, Flows of materials with yield. J. Rheol. 31 (1987), 385-404.

[23] A. O. Nieckele, M. F. Naccache and P. R. Souza Mendes, Crossflow of viscoplastic materials through tube bundles. J. Non-Newt. Fluid Mech. 75 (1998), 43-54.

[24] R. B. Bird, G. C. Dai and B. J. Yarusso, The rheology and flow of viscoplastic materials. Rev. Chem. Eng. 1 (1983), 1-70.

[25] Y. Zang, R. L. Street and J. R. Koseff, A non-staggered grid, fractional step method for time-dependent incompressible Navier-Stokes equations in curvilinear coordinates. J. Comp. Phys. 114 (1994), 18-33.

[26] C. J. Lawrence and G. M. Corfield, Non-viscometric flow of viscoplastic materials: squeeze flow. In *Dynamics of Complex Fluids*, M. J. Adams, R. A. Mashelkar, J. R. A. Pearson and A. R. Rennie (eds), Imperial College Press-The Royal Society (1998), 379-393.

mesh size	Bn	R	U
32×30	1.24	14.0	$7.48 \cdot 10^{-2}$
	1.25	19.4	$7.43 \cdot 10^{-2}$
	1.25	26.9	$7.41 \cdot 10^{-2}$
42×40	1.25	14.1	$7.40 \cdot 10^{-2}$
	1.26	19.4	$7.37 \cdot 10^{-2}$
	1.26	26.7	$7.35 \cdot 10^{-2}$
62×60	1.25	14.1	$7.40 \cdot 10^{-2}$
	1.26	19.4	$7.38 \cdot 10^{-2}$
	1.26	27.0	$7.37 \cdot 10^{-2}$
	1.26	42.2	$7.37 \cdot 10^{-2}$
62×60	4.25	90.5	$3.36 \cdot 10^{-2}$
	4.28	201	$3.33 \cdot 10^{-2}$
	4.3	449	$3.32 \cdot 10^{-2}$

Table 1: Effects of the regularization parameter R and number of mesh points on the computed cell-averaged velocity U for solid fraction $\phi = 0.1$. The yield surfaces for the cases $Bn = 4.28 \pm 0.03$ are shown in Figure 1.

Figure captions

Figure 1. Effects of the regularization parameter R on the yield surfaces, defined as the surfaces where $\Pi_\tau = \tau_0$. The solid fraction is $\phi = 0.1$, the Bingham number is $Bn = 4.28 \pm 0.03$; the mesh size is 62×60. Flow is from left to right. Yield surfaces are shown for $R = 449$, 201 and 90.5 (these cases are also shown in Table 1). The unyielded zones include the points of symmetry, and decrease in size with increasing values of R.

Figure 2. Contours of constant apparent viscosity for $\phi = 0.6$; $Bn = 22.4$, $R = 45.7$ (a) and $Bn = 1322$, $R = 991$ (b). The viscosity values used (where $\mu_B = 1$) are $0, 4.4, .., 44$ and $0, 98, .., 980$, respecitively.

Figure 3. Numerical results ($\bullet$) for the drag coefficient C_d of a cylinder in a square array as a function of the Bingham number Bn for solid area fractions, from bottom to top, 0.01, 0.1, 0.2, 0.3, 0.4, 0.5 and 0.6. The horizontal dotted lines represent the Newtonian values ($Bn = 0$). Also shown are the approximate asymptotic result (6) (solid line) and numerical simulation results for a single cylinder ($\square$) by Adachi & Yoshioka (1973); the dashed line is the correlation for a single cylinder obtained from numerical simulations by De Besses *et al.* [14].

Figure 4. Numerical simulation results for the difference between the drag coefficient C_d of a cylinder in a square array and that for a Newtonian fluid as a function of Bingham number Bn for area fractions 0.01 ($\square$), 0.1 (Δ), 0.2 (o), 0.3 ($\diamond$), 0.4 (∇), 0.5 ($+$) and 0.6 ($\triangleright$). Also shown ($\blacklozenge$) is C_d for flow at an angle of 45 degrees with respect to an axis of the array ($\phi = 0.3$).

Figure 5. Coefficient c_1 in (7) as a function of solid fraction ϕ: ($\square$), obtained from the numerical simulation data shown in Figure 3 by fitting second-order polynomials; (Δ), $\hat{c}_1$ obtained from the approximation (11) by extrapolating a scaling result for power-law fluids to $n = 0$. The solid and dashed lines are the lubrication theories (17) and (12) for biviscosity fluids and perfectly plastic materials, respectively. The dotted line is the approximate result (6) of Adachi & Yoshioka (1973) for a single cylinder.

Figure 6. Superficial fluid velocity U (divided by the corresponding Newtonian fluid value) as a function of dimensionless pressure gradient $2cG/\tau_0$. ($\Box$), $\phi = 0.1$; (Δ), $\phi = 0.3$; (o), $\phi = 0.6$. The lines represent (19).

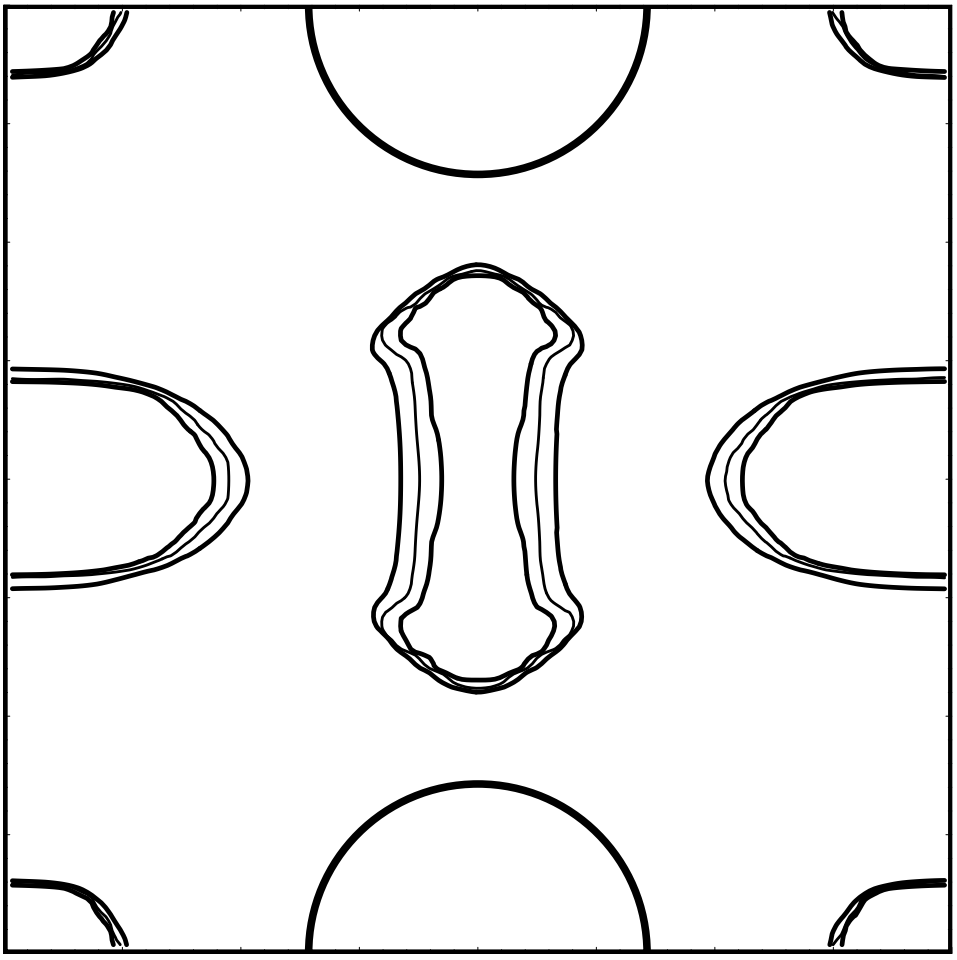

Fig. 1. Effects of the regularization parameter R on the yield surfaces, defined as the surfaces where $\Pi_\tau = \tau_0$. The solid fraction is $\phi = 0.1$, the Bingham number is $Bn = 4.28 \pm 0.03$; the mesh size is 62×60. Flow is from left to right. Yield surfaces are shown for $R = 449$, 201 and 90.5 (these cases are also shown in Table 1). The unyielded zones include the points of symmetry, and decrease in size with increasing values of R.

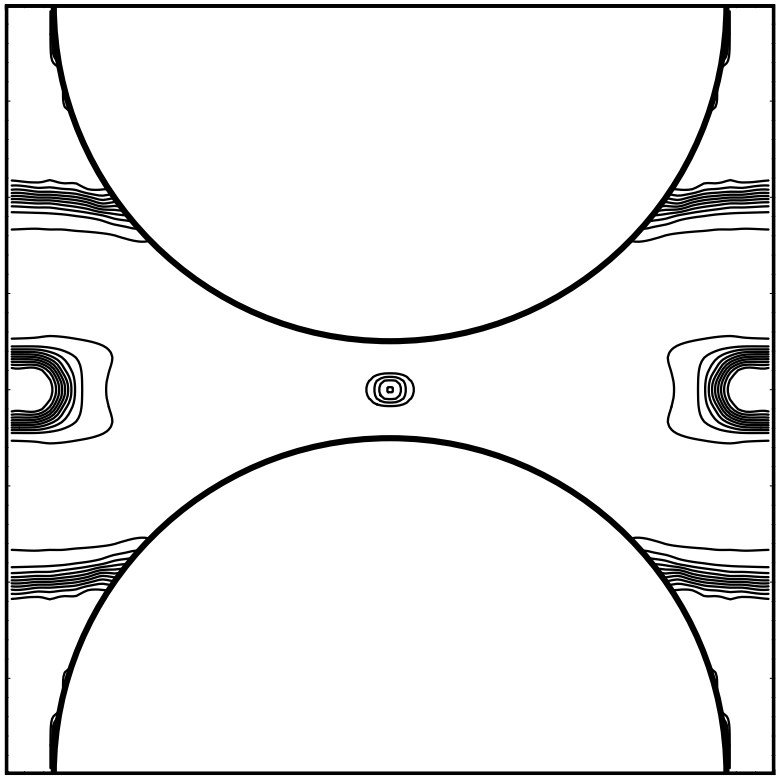

(a)

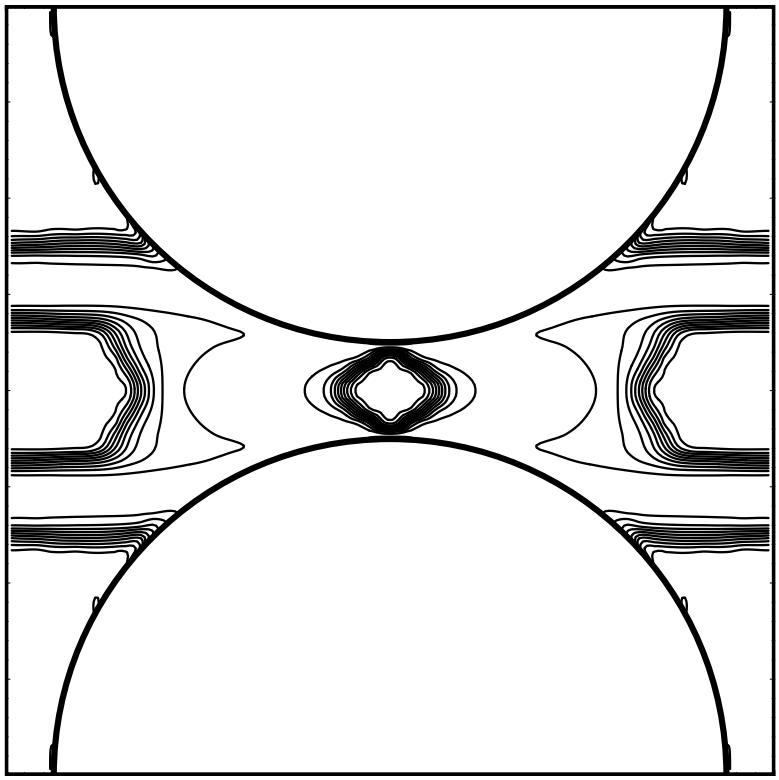

(b)

Fig. 2. Contours of constant apparent viscosity for $\phi = 0.6$; $Bn = 22.4$, $R = 45.7$ (a) and $Bn = 1322$, $R = 991$ (b). The viscosity values used (where $\mu_B = 1$) are $0, 4.4, .., 44$ and $0, 98, .., 980$, respecitively.

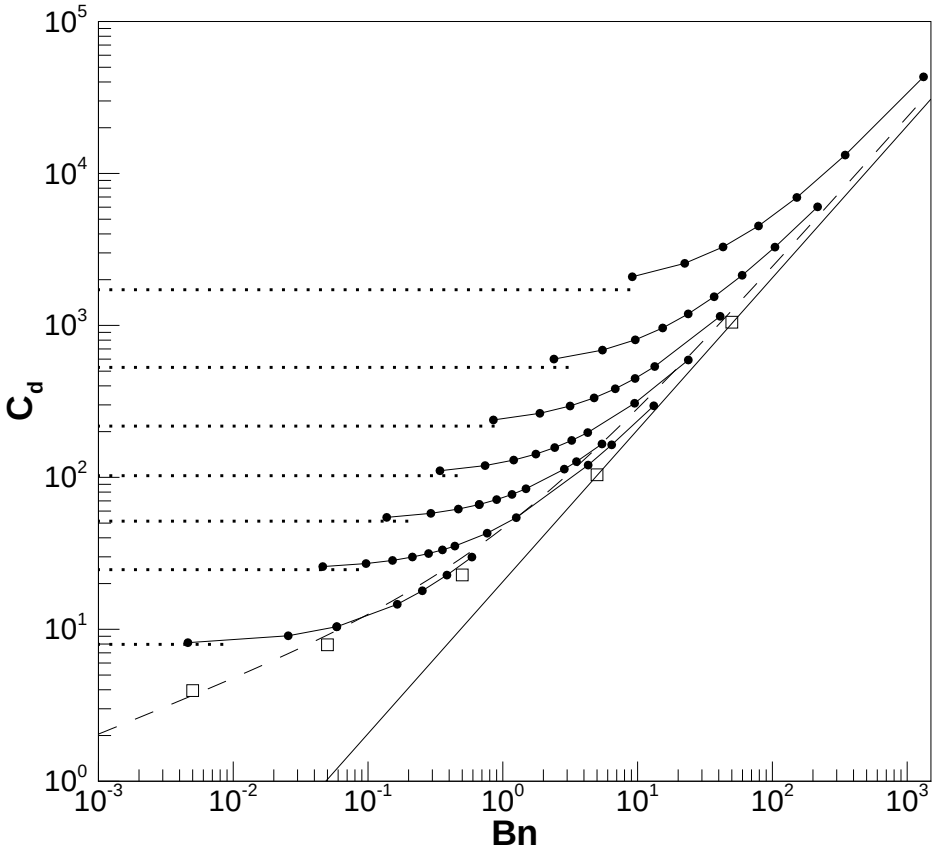

Fig. 3. Numerical results (•) for the drag coefficient C_d of a cylinder in a square array as a function of the Bingham number Bn for solid area fractions, from bottom to top, 0.01, 0.1, 0.2, 0.3, 0.4, 0.5 and 0.6. The horizontal dotted lines represent the Newtonian values ($Bn = 0$). Also shown are the approximate asymptotic result (6) (solid line) and numerical simulation results for a single cylinder (□) by Adachi & Yoshioka (1973); the dashed line is the correlation for a single cylinder obtained from numerical simulations by De Besses *et al.* [14].

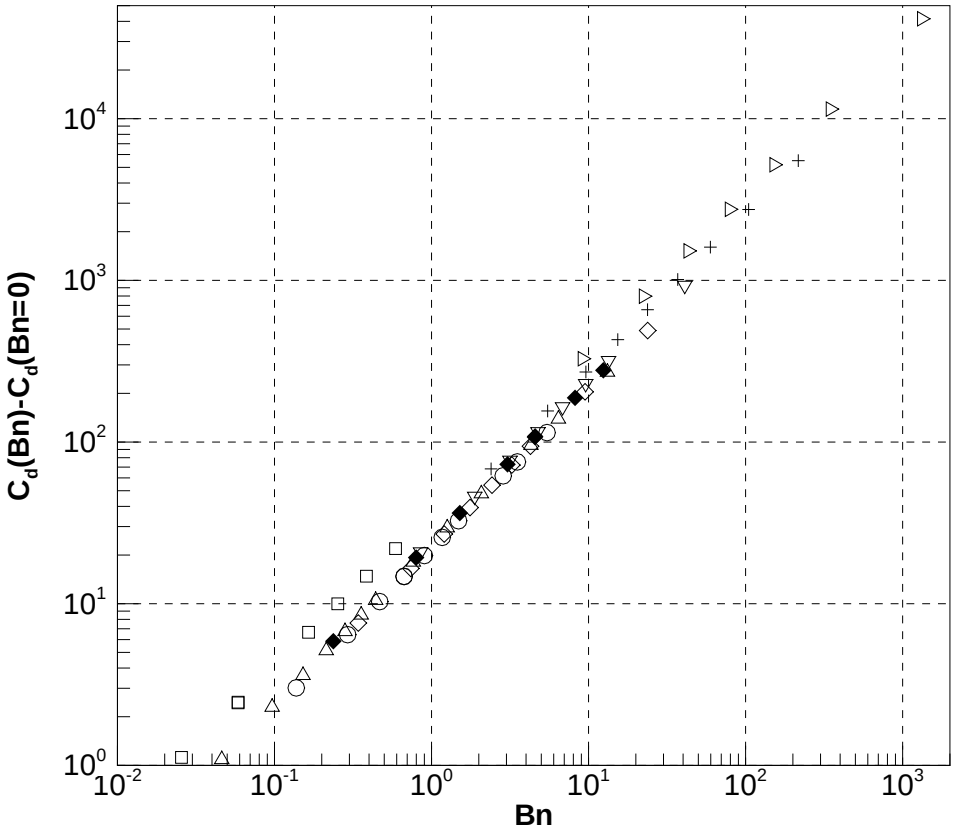

Fig. 4. Numerical simulation results for the difference between the drag coefficient C_d of a cylinder in a square array and that for a Newtonian fluid as a function of Bingham number Bn for area fractions 0.01 (□), 0.1 (Δ), 0.2 (o), 0.3 (⋄), 0.4 (∇), 0.5 (+) and 0.6 (▷). Also shown (⧫) is C_d for flow at an angle of 45 degrees with respect to an axis of the array ($\phi = 0.3$).

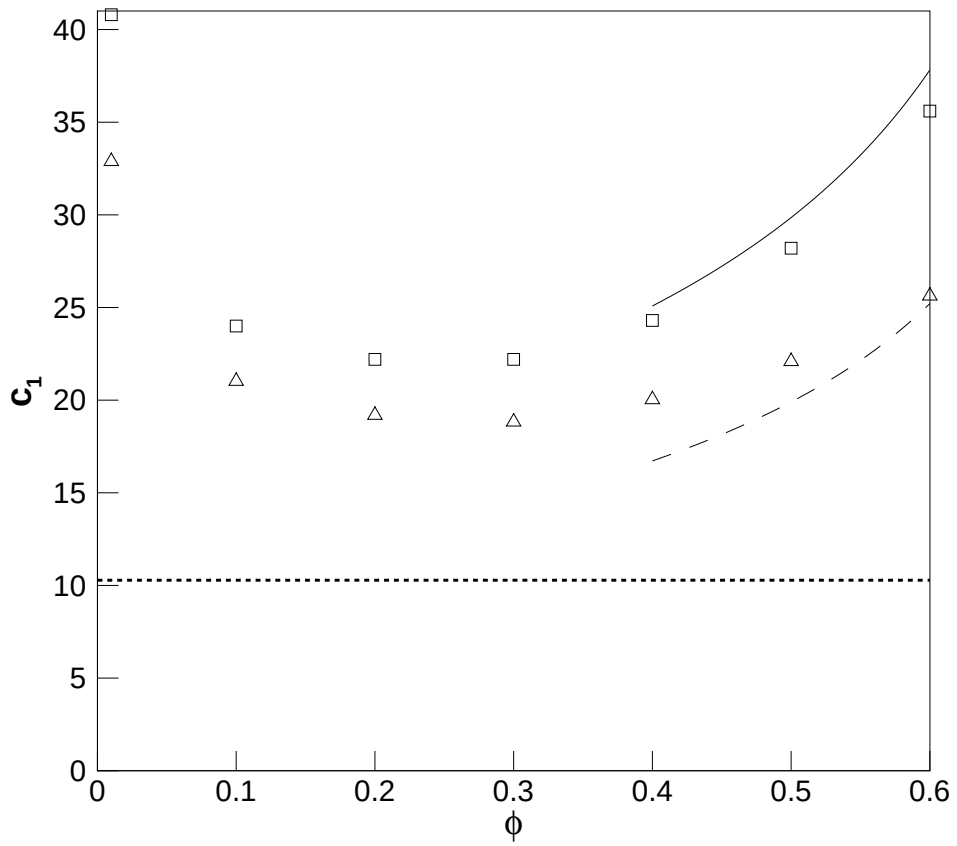

Fig. 5. Coefficient c_1 in (7) as a function of solid fraction ϕ: ($\Box$), obtained from the numerical simulation data shown in Figure 3 by fitting second-order polynomials; (Δ), $\hat{c}_1$ obtained from the approximation (11) by extrapolating a scaling result for power-law fluids to $n = 0$. The solid and dashed lines are the lubrication theories (17) and (12) for biviscosity fluids and perfectly plastic materials, respectively. The dotted line is the approximate result (6) of Adachi & Yoshioka (1973) for a single cylinder.

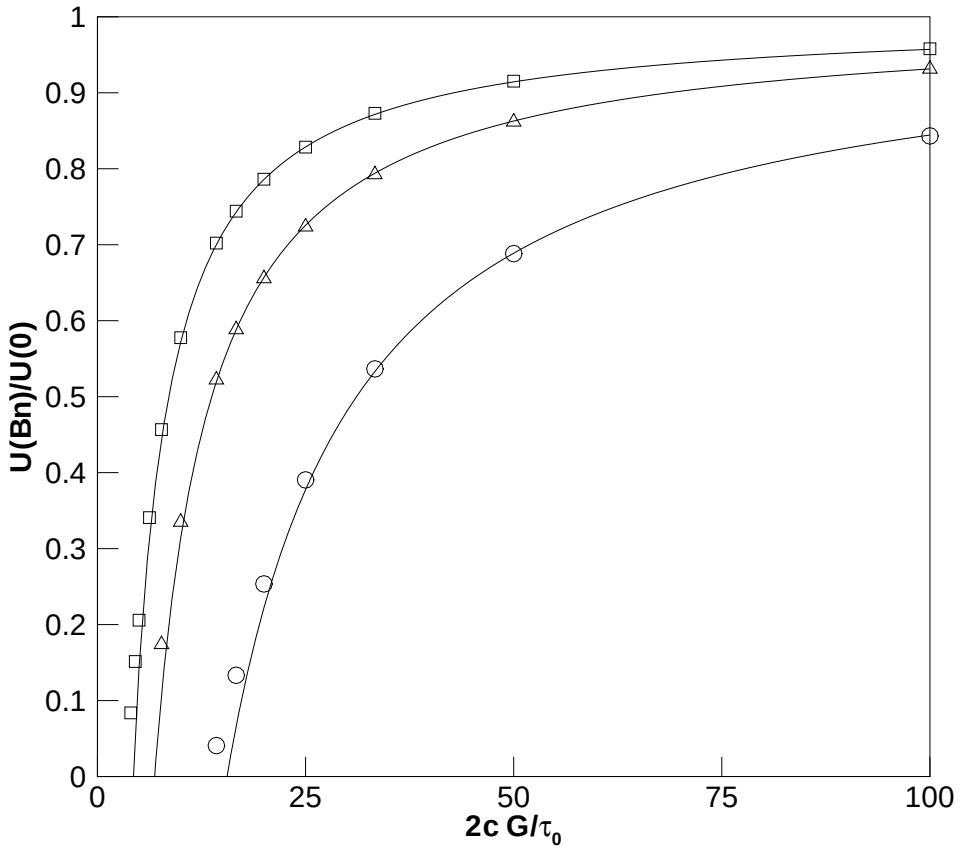

Fig. 6. Superficial fluid velocity U (divided by the corresponding Newtonian fluid value) as a function of dimensionless pressure gradient $2cG/\tau_0$. (□), $\phi = 0.1$; (Δ), $\phi = 0.3$; (o), $\phi = 0.6$. The lines represent (19).